Solutal convection instability caused by dissolution

Michael Berhanu, Julien Philippi, Sylvain Courrech Du Pont, Julien Derr

Physics of Fluids

Solutal convection instability caused by dissolution

Cite as: Phys. Fluids **33**, 076604 (2021); https://doi.org/10.1063/5.0052305
Submitted: 30 March 2021 . Accepted: 15 June 2021 . Published Online: 12 July 2021

Michael Berhanu, Julien Philippi, Sylvain Courrech du Pont, and Julien Derr

Physics of Fluids ARTICLE scitation.org/journal/phf

Solutal convection instability caused by dissolution

Cite as: Phys. Fluids **33**, 076604 (2021); doi: 10.1063/5.0052305
Submitted: 30 March 2021 · Accepted: 15 June 2021 ·
Published Online: 12 July 2021

Michael Berhanu,[1,a)] Julien Philippi,[1,2] Sylvain Courrech du Pont,[1] and Julien Derr[1]

AFFILIATIONS

[1]MSC, Université de Paris, CNRS (UMR 7057), 75013 Paris, France
[2]TIPs, Université Libre de Bruxelles, 1050 Bruxelles, Belgium

[a)]Author to whom correspondence should be addressed: michael.berhanu@univ-paris-diderot.fr

ABSTRACT

When a soluble solid body is suddenly put in contact with water, a convection flow can be generated. Once the fluid layer charged into solute is sufficiently dense, this layer becomes unstable under the action of the buoyancy forces. We perform here a linear stability analysis in order to predict the time of appearance of the convection flow, the onset time, and the associated wavelength. As the base state evolves with time due to the solute diffusion, the usual theoretical methods cannot be used. We show that the criterion of marginal instability with a "frozen base state" used for convection in porous media fails for providing the onset parameters in fluid convection. Here, using a modified criterion, i.e., the instability growth rate must be larger than the time evolution of the base state, we find the onset parameters in satisfying agreement with the previous experimental and numerical works. Our results complete our previous numerical work [J. Philippi *et al.*, "Solutal convection induced by dissolution," Phys. Rev. Fluids **4**, 103801 (2019)] in order to determine the conditions for generating a convective flow under the action of dissolution.

I. INTRODUCTION

Solutal convection instability constitutes a standard mechanism for generating macroscopic flows in the absence of mechanical forcing. A fluid area with a high concentration of solute is denser than surrounding less concentrated fluid. Due to gravity, a solutal convection flow can then appear. Literally analog to the thermal convection, where the density variations are caused by fluid thermal expansion, solutal convection can be triggered, for example, by the evaporation of water,[1,2] increasing the solute concentration at the top surface. Solutal convection is also of prime importance in geosciences. This phenomenon occurs, for example, not only in the shaping of magmatic chambers[3–5] but also for the chemical erosion of soluble rocks in geomorphology. Specifically, solutal convection can lead to the formation of dissolution cavities in the absence of an external flow in soluble minerals like salt,[6,7] gypsum,[8–10] and even in limestone caves[11] despite the very small saturation concentration. Solutal convection also has been extensively studied for Darcy flows in porous media especially in the context of CO_2 sequestration.[12–14] In the laboratory, solutal convection has also been investigated, when a soluble body (horizontal or inclined) is suspended in a initially quiescent bath of water.[15–19] On the bottom, the concentrated boundary layer detaches by emitting sinking plumes. The convection flows control the dissolution rate, which is constant with time[16,19,20] and leads to a patterning of the bottom face, by differential dissolution.[16,19] Despite the simplicity of the experimental configuration, these examples do not correspond to the classical Rayleigh–Bénard problem, where the initial base state is stationary. A fluid layer of a given height lies between two horizontal plates, each having a prescribed temperature for thermal convection or prescribed concentration for solutal convection. Here, first, there is no equivalent of the plate separation. The geometry in the fluid phase can be considered as semi-infinite. Second, due to the development of the concentration boundary layer by diffusion in a first step, the base state of the instability is time-dependent and the convective flow starts after a specific duration, the onset time t_{onset}. Then, the standard methods of linear stability analysis cannot be used to predict t_{onset}, the associated wavelength, and the growth-rate of the convective instability. One notes that in numerous practical cases, thermal convection generates a flow due to a time change of conditions. These situations do not correspond to the classic stationary Rayleigh–Bénard problem.

Several approaches have been proposed for time dependent convection in various configurations (thermal or solutal convection, Navier–Stokes equations, or Darcy flow): the frozen base state assumption,[21–24] the amplification theory,[25–27] the propagation theory,[28–30] the energy stability analysis,[31] and the non-normal linear stability analysis.[32–34] Whereas these methods provide some insights on the physical mechanisms, they rely on strong hypotheses and on arbitrary criteria defining the onset. They are thus difficult to compare with the experimental situations. Although not supported by a linear instability

analysis of the convection flow, Tan and Thorpe[35] propose a simple and pragmatic approach to determine the onset of non-stationary convection. They define a transient Rayleigh number based on the instantaneous temperature gradient $(\partial T)/(\partial z)$ and calculate its maximal value as a function of z. The onset time is determined, when the maximal transient Rayleigh number reaches the critical Rayleigh number established in the literature for a constant gradient (linear temperature profile) between two plates, i.e., a non-evolving base state. This method is appropriately tested and compared with experiments for thermal convection.

Recently, we reported in the article of Ref. 20 two dimensional numerical simulations of the solutal convection flow using Boussinesq approximations and a rigid top interface incorporating the solute flux due to dissolution. By carrying out a correlation analysis on the density profiles close to the interface, we determined the onset time t_{onset} and wavelength λ_{onset} for an extensive exploration of the parameters. Scaling laws were proposed and verified for fast and low chemical dissolution kinetics compared to the diffusion in the boundary layer. The fast dissolving regime is consistent with salt dissolution experiments, when the initial density of the bath is varied.

In this article, we complete that previous numerical work by a theoretical study of the onset of the solutal convection. By performing a linear stability analysis, we aim to determine the conditions of appearance of solutal convection and to determine as a function of the experimental parameters, the onset time, and the characteristic wavelength at the onset. Using a simplified description of solutal convection, we propose two linear stability analysis models. The first is valid for the large Schmidt number S_c (ratio of kinematic viscosity to the diffusion coefficient) only. The influence of the dissolution kinetic coefficient is also considered in the first model. The second model takes into account the fluid acceleration through a dependency with the Schmidt number S_c. To incorporate the temporal evolution of the base state, we propose a modified instability criterion: the instability growth rate must be larger than the time evolution of the base state. Contrary to the usual criterion of marginal instability for steady problems, this modified criterion provides the correct orders of magnitude.

II. THEORETICAL BACKGROUND AND BASIC SCALING

We use the same set of equations than in Ref. 20 in the same framework of hypothesis, and we recall here only the essential results. The physical problem can be understood as an advection–diffusion problem in the fluid, which is coupled with a moving solid boundary due to the dissolution/precipitation.[36] The dissolution reaction at the solid/liquid interface imposes an in-going flux as a boundary condition for the advection–diffusion equation of the solute mass concentration $c(\boldsymbol{r}, t)$. We assume that the flux is proportional to the distance to the thermodynamic equilibrium, i.e., the difference between the saturation concentration c_{sat} and the solute molecular concentration at the interface c_i (z_i being the position of a point at the interface). α is a positive coefficient with the dimension of a velocity, which accounts for the kinetics of the chemical dissolution reaction and is sometimes called the dissolution rate. When dissolving, by the mass conservation principle, the solid interface displaces. For a small saturation concentration compared to the liquid density, the time evolution of the interface remains large compared to the time change of the hydrodynamics, defining a quasi-static regime. The advection flux of solute can be neglected at the interface, leading to a simplified dissolution boundary condition. Then, the erosion velocity $\boldsymbol{v_d}$ corresponding to the motion of the liquid–solid boundary multiplied by the solid density ρ_s equals this chemical flux and also the diffusion solute flux at the boundary of the liquid domain (always for small enough $\boldsymbol{v_d}$)

$$\rho_s \boldsymbol{v_d} \cdot \boldsymbol{n} = \alpha\,(c_{sat} - c_i) = D\,\boldsymbol{\nabla} c|_i \cdot \boldsymbol{n}. \tag{1}$$

Here, $\boldsymbol{n}$ is the normal vector to the interface directed outward from the liquid. D is the diffusion coefficient of the solute in the liquid phase, and it is supposed to be independent of the concentration in the first approximation. (This hypothesis is acceptable for salt and most of ionic solids but strongly false for some organic compounds like sugar.) We suppose also a linear relation between the concentration $c(x, z, t)$ and the density field $\rho(x, z, t)$

$$\rho = \rho_0 + (\rho_{sat} - \rho_0)\,\frac{c}{c_{sat}}, \tag{2}$$

with ρ_0 being the density of fresh water and ρ_{sat} being the density when the concentration equals the saturation concentration c_{sat}. In this work, we neglect the motion of the dissolving interface. The hypothesis is valid for most practical cases to study the short time hydrodynamics, which adapts quasi-instantaneously to the new boundaries of the fluid domain.

We consider a fixed two-dimensional domain O_{xz} [see Fig. 1(a)], with $-H_z < z < 0$, filled with the liquid, in which a solute is dissolving from the top boundary $z = 0$. Qualitatively as illustrated in Fig. 1(b), during a first step, the dissolution brings solute at the vicinity of the interface. This concentrated area defines a solute boundary layer. The thickness δ of this boundary layer grows by diffusion, until it reaches a critical value at $t = t_{onset}$, where due to the action of gravity, this layer destabilizes, generating a convective flow. The objective of this article is to evaluate theoretically by a linear stability analysis the onset time t_{onset} and the associated wavelength λ_{onset}, which is also related to the critical boundary layer thickness. After a duration of order few onset times, we reach a quasi-stationary regime where the convection is said turbulent,[16,20] which is out of the validity range of the linear stability analysis. Plumes are emitted intermittently, and the concentration boundary layer thickness is in average constant, which implies a constant dissolution rate.

In the domain [see Fig. 1(a)], we study the concentration field $c(x, z, t)$ and the fluid velocity $\boldsymbol{u}(x, z, t) = (u, w)$. The horizontal extension is supposed infinite. The boundary conditions are for the velocity field $\boldsymbol{u}(z = 0) = 0$, $\boldsymbol{u}(z = -H_z) = 0$ and for the concentration field $(\partial c/\partial z)|_{z=-H_z} = 0$, and at the solid/liquid dissolving interface, the specific dissolution boundary condition

$$\alpha\,(c_{sat} - c_i) = D\,(\partial c/\partial z)|_{z=0}. \tag{3}$$

Although the domain is static in this approach, this boundary condition for $c(x, z, t)$ involves simultaneously c_i and its derivative $\boldsymbol{\nabla} c|_i$ and is thus non-classic. At $t = 0$, the concentration and the velocity field are zero. In a first step, the solute concentration is carried out from the dissolving boundary, which imposes a variable solute flux.

For this boundary condition given in Eq. (3), when the interface is motionless, John Crank provides an analytic solution of the solute diffusion equation in a semi-infinite domain (Ref. 37, Sec. 3.3.1)

$$c = c_{sat}\left[\operatorname{erfc}\left(\frac{-z}{2\sqrt{Dt}}\right) - \exp\left(-\frac{z}{\mathscr{L}} + \frac{Dt}{\mathscr{L}^2}\right)\operatorname{erfc}\left(-\frac{z}{2\sqrt{Dt}} + \frac{\sqrt{Dt}}{\mathscr{L}}\right)\right], \tag{4}$$

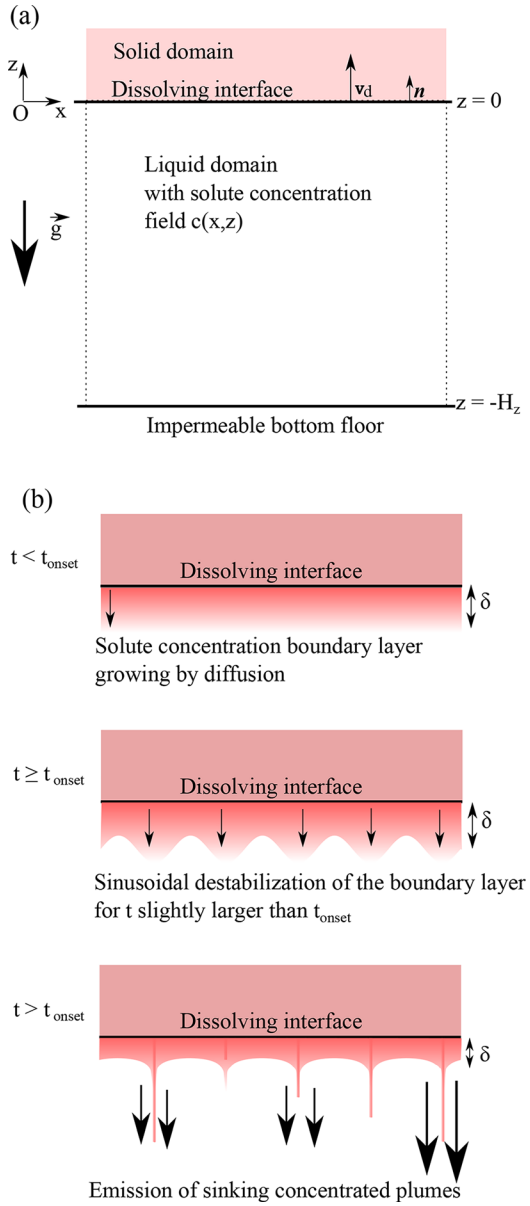

FIG. 1. (a) Schema of the domain on which the solutal convection instability is analyzed. (b) Schema of the instability near the dissolving interface. Before the onset time t_{onset}, the concentration boundary layer of thickness δ grows by diffusion. Just after t_{onset}, due to the action of gravity, the convection starts and the boundary layer adopts a sinusoidal shape with a wavelength λ_{onset}. The purpose of the linear stability analysis is to predict the values of t_{onset} and λ_{onset}. After a few onset times, due to the nonlinear terms, plumes that are concentrated into solute are emitted toward the bottom. A turbulent regime is quickly reached as the position and the duration between two successive plumes are strongly fluctuating.

where $\mathscr{L} = D/\alpha$ is a characteristic length and erfc is the complementary error function. For a large enough distance from the boundary, $|z| \gg \mathscr{L}$, the concentration profile is well described by the simpler function: $c = c_{sat}\,\mathrm{erfc}(-z/(2\sqrt{D\,t}))$, which corresponds to the solution of the diffusion equation when $c(z=0) = c_{sat}$. Considering that the characteristic spatial scale of the problem is the concentration boundary layer thickness δ, we introduce the dimensionless Damköhler number $D_a = (\alpha\,\delta)/D = \delta/\mathscr{L}$. For salt in water with $\alpha = 5.0 \times 10^{-4}$ m s^{-1} (Ref. 38) and $D = 1.61 \times 10^{-9}$ m^2 s^{-1} (saturated brine[39]), $\mathscr{L} = 3.2 \times 10^{-6}$ m. The estimation of δ will show that D_a is then large in front of one. This example corresponds to a fast dissolving case, where the dissolution rate is limited by the solute transport and not by the chemical kinetics. By taking the limits $D_a \gg 1$ and $z \to 0$ in Eq. (4), one can show that the top boundary condition is approximated to $c(z=0) \approx c_{sat}$.

In the fluid phase, the solute is transported by the flow. The standard methods to address thermal convection[40] can be used for solutal convection by replacing the temperature field by the concentration field. For small enough solute concentration, we can use the Boussinesq approximation,[40] i.e., the variations of ρ with c are only considered for the gravity term. We assume also an incompressible flow. The hydrodynamics and the solute advection are then described by the equations, where $\nu = \mu/\rho_0$ is the kinematic viscosity,

$$\nabla \cdot \boldsymbol{u} = 0,$$
$$\frac{\partial c}{\partial t} + (\boldsymbol{u}\cdot\boldsymbol{\nabla})c = D\triangle c,$$
$$\rho_0\left(\frac{\partial \boldsymbol{u}}{\partial t} + (\boldsymbol{u}\cdot\boldsymbol{\nabla})\boldsymbol{u}\right) = -\boldsymbol{\nabla}P - \rho(c)\,g\,\boldsymbol{e_z} + \nu\,\rho_0\,\triangle\boldsymbol{u}\,.$$

The spatial variations of diffusion coefficient D and of the kinematic viscosity ν with the concentration field are neglected. After removing the hydrostatic part of the pressure and after appropriate nondimensionalization where the distances are rescaled by a length L, the times by the diffusive timescale L^2/D, and the concentrations by the saturation concentration c_{sat}, one obtains

$$\frac{\partial c^*}{\partial t^*} + (\boldsymbol{u}^*\cdot\boldsymbol{\nabla}^*)c^* = \triangle^* c^*, \tag{5}$$

$$\frac{\partial \boldsymbol{u}^*}{\partial t^*} + (\boldsymbol{u}^*\cdot\boldsymbol{\nabla}^*)\boldsymbol{u}^* = -\boldsymbol{\nabla}^* P^* - S_c\,R_a\,c^*\,\boldsymbol{e_z} + S_c\,\triangle^*\boldsymbol{u}^*, \tag{6}$$

with $S_c = \nu/D$, the Schmidt number (about 1000 for salt) and $R_a = \frac{\beta\,g\,L^3}{\nu D}$, the Rayleigh number. $\beta = (\rho_{sat} - \rho_0)/\rho_0$ is the density contrast, which depends on the density for the saturation concentration. The boundary condition at the dissolving boundary [Eq. (3)] reads in a dimensionless form in the fluid phase with $\alpha^* = (\alpha\,L)/D$

$$\alpha^*\,(c^* - 1) = -\boldsymbol{\nabla}^* c^*\cdot\boldsymbol{n}. \tag{7}$$

In a stationary regime, for the classic Rayleigh–Bénard problem by choosing L as the distance between the two horizontal plates (the vertical system size), the convective flow appears, when R_a exceeds a critical value depending on the boundary conditions: $R_{ac} = 27\,\pi^4/4 \approx 657.5$ for free-surface boundaries, $R_{ac} = 1708$ for solid walls, and $R_{ac} = 1101$ for mixed conditions.[40] The corresponding wavelengths at the instability threshold are, respectively, $2.8\,L$, $2.0\,L$, and $2.3\,L$.

Here, the situation is more difficult to approach as the geometry is semi-infinite and the base state is time dependent. To model the experiments, we suppose indeed that at $t = 0$, the block is put in contact with water and initially the velocity and concentration fields are zero. In a first step, the solute diffuses from the solid interface and the velocity field remains zero. When the boundary layer reaches a large

enough thickness, it becomes unstable to the gravity and a convective flow starts. A simple criterion of convection onset consists thus to build the Rayleigh number on this length scale. The following scaling for the critical boundary layer thickness δ_c and the wavelength at onset λ_{onset} is obtained, using, for example, the mixed conditions ($R_{ac} = 1101$)[16,20]

$$\delta_c \approx Ra_c^{1/3}\left(\frac{\nu D}{\beta g}\right)^{1/3} \approx 10.33\left(\frac{\nu D}{\beta g}\right)^{1/3}, \tag{8}$$

$$\lambda_{onset} \approx 2.3\delta_{onset} \approx 23.75\left(\frac{\nu D}{\beta g}\right)^{1/3}. \tag{9}$$

As the boundary layer grows by diffusion during the first step, the onset time of convection scales as $t_{onset} = \delta_c^2/D$, and we get this last scaling

$$t_{onset} = K\left(\frac{\nu}{\beta g\sqrt{D}}\right)^{2/3}, \tag{10}$$

with the prefactor $K \approx Ra_c^{2/3} = 106.62$. These simple scaling are valid for large D_a and do not take into account the geometry of the boundary layer neither its dynamics, that is why they provide only the order of magnitude. In Ref. 20, we perform an experimental determination of t_{onset} for the dissolution of salt in the water bath with varying initial salt concentrations. We verify the scaling law [Eq. (10)], but the prefactor K differs by a factor 8 from the experiment, where $K \approx 12.8$. Using fresh water, the first plumes are emitted at $t \approx 1$ s. The onset time, when the boundary layer starts to deform, is thus smaller and t_{onset} is of order 0.5 s. In the same work, we carry out a numerical simulation of the convection flow in two-dimension and using the Boussinesq approximation. We also find in the conditions of salt dissolution by fresh water, larger values: $t_{onset} \approx 1.02$ s and a prefactor $K \approx 29.5$.

In the slow dissolution kinetic regime ($D_a \ll 1$), the previous reasoning to determine the scaling laws is no longer valid. As the value of the coefficient α matters now, the strength of convection would be characterized at least by the Rayleigh number and the Damkhöler number. By estimating the density at the dissolving interface as a function of D_a, the corresponding scaling for $D_a \ll 1$ can be derived (see Ref. 20)

$$\delta_{onset} \sim \left(\frac{D^2\nu}{\alpha\beta g}\right)^{1/4} \quad \text{and} \quad \lambda_{onset} \approx 2.3\,\delta_{onset}, \tag{11}$$

$$t_{onset} \sim \sqrt{\frac{\nu}{\alpha\beta g}}. \tag{12}$$

One can notice that the onset time is independent of the diffusion coefficient and grows to infinity as α is going to zero. The dissolution kinetics is in this case the limiting factor in solute transport.

III. LINEAR STABILITY ANALYSIS: FIRST MODEL AT LARGE SCHMIDT NUMBER

A. Model

To get a better understanding of the convection instability and of the onset prediction, we propose a linear stability analysis. We adapt earlier theoretical works performing a linear stability analysis of convection with a time-dependent base state for the concentration field, which is an unsteady solution of the diffusion equation in the absence of flow. Often, its temporal variation is supposed sufficiently slow compared to the growth rate of the instability; this is the hypothesis of a frozen base state. It was used for solutal convection in the porous media in the context of carbon dioxide sequestration, taking into account the dissolution kinetics[41] or not.[22,24] We restrict first our analysis to the case of large Schmidt number S_c, valid for salt dissolution, i.e., $S_c \gtrsim 100$. The method used for this linear stability analysis consists first in defining the time-dependent base state. After linearizing Eqs. (5) and (6), one considers then the time evolution of small perturbations of this base state. The perturbations are usually decomposed into normal modes, each corresponding to a distinct horizontal wavenumber, with the hypothesis of translation invariance along the horizontal coordinate x. Each mode has a specific structure as a function of z, which for a finite system size H_z can be decomposed into the Fourier series. The results are then extrapolated to a semi-infinite domain, by taking the limit of large H_z. The time evolution of each mode is described by a matrix system of the vertical Fourier modes. Usually, the instability domain corresponds to the values of parameters and wavenumbers for which the growth rate is positive. This is the marginal instability criterion, for which infinitesimal perturbations are amplified.

We consider the 2D domain O_{xz} depicted in Fig. 1, with $-H_z < z < 0$, filled with the liquid phase, in which the solute penetrates by dissolution in the upper boundary in $z = 0$. The horizontal dimension is infinite. To use the previous set of dimensionless equations, we choose the scale $L = H$ for which $R_a = 1$. Then, the dimensionless system height $\mathscr{H}$ is defined by $H_z = \mathscr{H} \times H$. The solute transport and the fluid motion are described in Eqs. (5) and (6). For clarity, we omit the * superscript. The top and the bottom boundaries are impermeable for the velocity field $\mathbf{u}(0)\cdot\boldsymbol{e_z} = \mathbf{u}(-\mathscr{H})\cdot\boldsymbol{e_z} = 0$. The concentration flux is zero at the bottom $\frac{\partial c}{\partial z}|_{z=-\mathscr{H}} = 0$, but at the top boundary, the concentration flux is ruled by the dissolution condition written in a dimensionless form in Eq. (7). Initially, at $t = 0$, the concentration and velocity fields are zero.

The first step of the method consists in determining the evolving base state for the concentration field $c_b(z,t)$, which is the solution of the diffusion equation [Eq. (5) with $u = 0$]. For a large system size, we can adopt the solution for a semi-infinite system [Eq. (4)] in a dimensionless form

$$c_{b,C}(z,t) = \left[\operatorname{erfc}\left(-\frac{z}{2\sqrt{t}}\right) - \exp\left(-D_a z + D_a^2 t\right)\operatorname{erfc}\left(-\frac{z}{2\sqrt{t}} + D_a\sqrt{t}\right)\right], \tag{13}$$

with $D_a = \alpha H/D$ being the Damkhöler number built with the scale H. If we consider the limit of fast dissolution kinetics, $D_a \gg 1$ (justified for salt dissolution) where $c(z=0,t) = c_{sat}$, an exact solution of the diffusion equation for any system size can be derived by doing a Fourier decomposition in z[22,24]

$$c_{b,S}(z,t) = 1 + \sum_{n=1}^{\infty}\left[\frac{4}{(2n-1)\,\pi}\exp\left(-\left[\frac{(2n-1)\pi}{2\mathscr{H}}\right]^2 t\right) \times \sin\left(\frac{(2n-1)\pi z}{2\mathscr{H}}\right)\right]. \tag{14}$$

While the diffusion front has not approached the bottom boundary, this last solution is well approximated by a simpler solution: $c_{b,E} = \mathrm{erfc}(-z/(2\sqrt{t}))$, using the complementary error function erfc. In the rest, we will investigate successively the two cases for the base state $c_b = c_{b,S}$ (solution of the diffusion equation at large D_a for a finite size system), and then $c_b = c_{b,C}$ (solution of the diffusion equation valid for all values of D_a and for a semi-infinite system).

Then the system of equation is linearized in the vicinity of the base state to consider the evolution of infinitesimal perturbations of the concentration $c'(x,z,t) = c - c_b$ and of the velocity field $\boldsymbol{u}(x,z,t) = u(x,z,t)\,\boldsymbol{e_x} + w(x,z,t)\,\boldsymbol{e_z}$. The pressure field is eliminated by taking the double curl of Navier–Stokes equations, which gives only a dependency on the vertical velocity w[40] with $\triangle_1 = \frac{\partial^2}{\partial x^2}$

$$\frac{\partial c'}{\partial t} - \triangle c' = -w\frac{\partial c_b}{\partial z}, \tag{15}$$

$$\frac{1}{S_c}\frac{\partial \triangle w}{\partial t} - \triangle(\triangle w) = -\triangle_1 c'. \tag{16}$$

The horizontal fluctuations are decomposed into normal modes of wavenumber k, and we examine the behavior of each mode separately. We assume perturbations of the form

$$c'(x,z,t) = \int [\tilde{c}(z,t)\ \exp(\imath k x) + c.c.]\,\mathrm{d}k,$$
$$w(x,z,t) = \int [\tilde{w}(z,t)\ \exp(\imath k x) + c.c.]\,\mathrm{d}k,$$

with $c.c.$ being the complex conjugate.

We thus obtain

$$\frac{\partial \tilde{c}}{\partial t} = -\tilde{w}\frac{\partial c_b}{\partial z} + \frac{\partial^2 \tilde{c}}{\partial z^2} - k^2\,\tilde{c}, \tag{17}$$

$$\frac{1}{S_c}\frac{\partial}{\partial t}\left(\frac{\partial^2 \tilde{w}}{\partial z^2} - k^2\,\tilde{w}\right) = \frac{\partial^4 \tilde{w}}{\partial z^4} - 2k^2\frac{\partial^2 \tilde{w}}{\partial z^2} + k^4\,\tilde{w} + k^2\,\tilde{c}. \tag{18}$$

Similarly to the work of Slim and Ramakrishnan,[24] we look for solutions of $\tilde{c}$ and $\tilde{w}$ under the form of Fourier series in z truncated at the order N for the mode of wavenumber k

$$\tilde{c}(z,t) = \sum_{n=1}^{N} \gamma_n(t)\ \sin\left(\frac{(2n-1)\pi z}{2\mathscr{H}}\right), \tag{19}$$

$$\tilde{w}(z,t) = \sum_{n=1}^{N} \omega_n(t)\ \sin\left(\frac{n\pi z}{\mathscr{H}}\right). \tag{20}$$

These expressions verify the boundary conditions for c and w, but not the non-slip condition for u expected for a viscous fluid in contact with a solid surface, because the horizontal velocity is derived using $\boldsymbol{\nabla}\cdot\boldsymbol{u} = 0$, which imposes $w(z=0) = \frac{\partial w}{\partial z}|_{z=0} = 0$[40] and thus is not compatible with a Fourier series decomposition. However, we pursue with these expressions, Eqs. (19) and (20), which describe satisfyingly the physics at play but can possibly underestimate the predicted onset times.

We neglect the inertial term in the limit $S_c \gg 1$, and we use the Galerkin method that projects the concentration and the vertical velocity fields on a discrete spatial Fourier base. Equation (17) is multiplied by Eq. (20), whereas Eq. (18) is multiplied by Eq. (19). The results are integrated with respect to z between $-\mathscr{H}$ and 0. The products imply us to consider both a sum of index $n \in [1,N]$ and another of index $m \in [1,N]$. Using the properties of orthogonality of the Fourier base, the results can be considerably simplified and the variable w can then be eliminated. As in Ref. 24, we then write the linearized system derived from Eqs. (17) and (18) under a matrix differential linear equation for a given system size $\mathscr{H}$, time t, and wavenumber k: $\frac{dV}{dt} = A(t)\,V$ with $V = (\gamma_1,\ldots,\gamma_N)^\top$ ($\top$ designates the transpose operation). The elements of matrix A are computed from the system in the limit $S_c \gg 1$ under the form: $A = B - C\,E^{-1}\,D$. In the case $c_b = c_{b,S}$ (fast dissolution kinetics), the coefficients are exactly (see the Appendix)

$$B_{mn} = -\left[k^2 + \left(\frac{(2n-1)\pi}{2\mathscr{H}}\right)^2\right]\delta_{mn},$$

$$C_{mn} = \frac{1}{\mathscr{H}}\left[\exp(-[(m+n-1/2)\pi/\mathscr{H}]^2\,t) - \exp(-[(m-n-1/2)\pi/\mathscr{H}]^2\,t)\right],$$

$$D_{mn} = \frac{k^2}{\pi}(-1)^{m+n}\,\frac{4m}{4m^2-(2n-1)^2},$$

$$E_{mn} = \frac{1}{2}\left[k^4 + \left(\frac{n\pi}{\mathscr{H}}\right)^4 + 2k^2\left(\frac{n\pi}{\mathscr{H}}\right)^2\right]\delta_{mn}.$$

In the case $c_b = c_{b,C}$ (the dissolution kinetics is taken into account for a large enough system), the coefficients are the same except for C_{nm}, which are computed by numerical integration

$$C_{nm} = \frac{-2}{\mathscr{H}}\int_{-\mathscr{H}}^{0} \frac{\mathrm{d}c_{b,C}}{\mathrm{d}t}\,\sin\left(\frac{n\pi z}{\mathscr{H}}\right)\sin\left(\frac{(2m-1)\pi z}{2\mathscr{H}}\right)\mathrm{d}z\,.$$

If σ, the largest real part of the eigenvalues of the matrix A is positive, then fluctuations are amplified, the system is unstable, and the convection must start. The corresponding concentration perturbation must grow exponentially in time (like $\mathrm{e}^{\sigma t}$), and the spatial shape of this perturbation is given by the corresponding eigenvector. We obtain a criterion of marginal instability, for the shortest time t_{onset} and the first wavenumber k_{onset} for which $\sigma > 0$. However, as it will be presented in Sec. III B, the orders of magnitude are inconsistent with the experimental results. Among the simplifying hypotheses, the use of the marginal instability criterion with a frozen base state appears invalid for convection in fluids modeled with the Navier–Stokes equations contrary to the convection in porous media described with the Darcy equation.[22,24,41,42] Therefore, we adopt a new instability criterion (the *modified instability criterion*), which supposes that the fluctuations must have a growth rate larger than the evolution of the base state. Physically, the fluctuations must grow faster than the diffusion front advances, so that the boundary layer emits plumes. For this model, it means that the largest real eigenvalue verifies $\sigma > \max_z\left(\frac{\partial c_b}{\partial t}\right)$. This criterion constitutes a sufficient condition to observe the development of a convection flow.

The modified instability criterion can be computed analytically for $c_{b,E} = \mathrm{erfc}(-z/(2\sqrt{t}))$, which constitutes a good approximation of $c_{b,S}$ at short time, as long as the diffusion front has not reached the bottom surface. The maximum of $(\partial c_{b,E}/\partial t)$ is found analytically to be as a function of time: $\frac{\mathrm{e}^{-1/2}}{\sqrt{2\pi\,t}} \approx \frac{0.24}{t}$. We note that this criterion provides results very close from those derived using the *relative* instability criterion:[43–45]

$\sigma > (1/||c_b||) \times (\mathrm{d}||c_b||/\mathrm{d}t)$ with $||c_b|| = [\int_{-\infty}^{0} c_b^2 \, \mathrm{d}z]^{1/2}$. This condition is better established mathematically and gives for $c_b = c_{b,E}$, $\sigma > 1/(4\,t) = 0.25/t$. For $c_b = c_{b,S}$, we again use as an approximate instability criterion $\sigma > 0.24/t$. When the dissolution kinetics must be taken into account, the criterion is computed numerically for $c_{b,C}$. We thus define the corresponding new onset time t_{onset} and wavenumber k_{onset} for the fastest growing k-mode overtaking the base state growth.

B. Results

We now present the results of the linear stability analysis, obtained with the function *eig* of MATLAB. We found that the computations converge for a number of $z-$ modes N of order of $\mathscr{H}$. We start in order to limit the computing time with $\mathscr{H} = 50$. To facilitate the discussion and the comparison with experiments, we present the results into dimensional units. The length scale H is chosen as $R_a = 1$, which gives for the parameters of salt ($\beta = 0.2$, $D = 1.61 \times 10^{-9}$ m^2 s^{-1}, and $\nu = 1.66 \times 10^{-6}$ m^2 s^{-1}),[19,20] $H \approx 1.11 \times 10^{-5}$ m. The corresponding timescale is then $H^2/D \approx 7.63 \times 10^{-2}$ s. The vertical size of the system is thus $H_z = \mathscr{H}\, H \approx 0.55$ mm.

In Fig. 2, we present the values σ of the largest eigenvalue, which identifies to the growth rate of the convective instability, as a function of time and wavenumber. We start with the case $c_b = c_{b,S}$ (fast dissolution kinetics) in (a). As expected, at short time σ is always negative and becomes positive after, which is depicted by the red curve. However, the criterion of marginal instability provides onset times and onset wavenumbers that appear too small compared to the experimental values. By adopting the modified criterion, the values are notably increased to be order of 0.2 s. The wavelength of the instability corresponds to the minimum of the black curve [bounding the domain where $\sigma(t,k) > \frac{\partial c_b}{\partial t}$] for the shortest time and a maximum of σ as a function of k. We remark that this instability domain is, however, very flat in k and that the instability may be weakly selective in wavelengths around $\lambda \approx 1$ mm. In Fig. 2(b), we plot the same colormap of σ in the case $c_b = c_{b,C}$ with $\alpha = 3.63 \times 10^{-6}$ m s^{-1} (the order of magnitude for gypsum dissolution[46]). This case corresponds to a Damkhöler number $D_a \approx 1.25$ (non-negligible dissolution kinetics) (with $D = 1.61 \times 10^{-9}$ m^2 s^{-1} and the vertical system size H_z as a characteristic length). We observe that the instability onset time is delayed and that the corresponding wavelength is slightly larger. The amplitude of the growth rates is significantly reduced.

The largest eigenvalue defines the most unstable mode. The spatial shape of this mode can be determined by computing numerically the corresponding eigenvector for t_{onset} and k_{onset}. This eigenvector is a linear combination of the z-Fourier modes. In Fig. 3, we show then in dimensionless units the spatial shape of the most unstable modes at the onset time for the perturbed concentration field $c'(x,z)$, using the modified instability criterion, for both base states $c_{b,S}$ and $c_{b,C}$. We observe that $c'(x,z)$ is zero in $z=0$, has a maximum close to this boundary, and decreases slightly with $-z$. Nevertheless, the size of the cavity $H_z = 50\,H \approx 0.55$ mm appears too small, because it is of the same order of magnitude than the instability wavelength. In this example, the convective boundary layer has the same size than the cavity, which limits the extrapolation toward a semi-infinite system.

Then, we test the dependency with α for several base state profiles $c_{b,C}$, and we compare the results with $c_{b,S}$, which does not take into account the dissolution kinetics for both the marginal instability criterion and the modified instability criterion. As it will be shown later, the first criterion gives results that are not consistent with experimental results and strongly depending on the domain size. Therefore, we discuss here only the results from the modified instability criterion. We find in Fig. 4 for strong values of α identical results for $c_{b,C}$ and $c_{b,S}$. Then the results differ for $\alpha < 10^{-4}$ m s^{-1}, which corresponds to a Damkhöler number built on the rescaling length H smaller than $D_a = 0.69$. This transition occurs, when t_{onset} becomes larger than the characteristic dissolution time D/α^2, which is the typical time needed for the concentration to reach c_{sat} at the dissolving boundary. In the slow dissolution kinetics regime, t_{onset} increases significantly when α decreases, as well as λ_{onset} but on a smaller variation range. The scaling drawn at the end of Sec. II is tested for small α values in black dashed lines. t_{onset} follows reasonably Eq. (12). Both scaling at low D_a were also verified in our numerical simulations.[20] In the fast dissolving

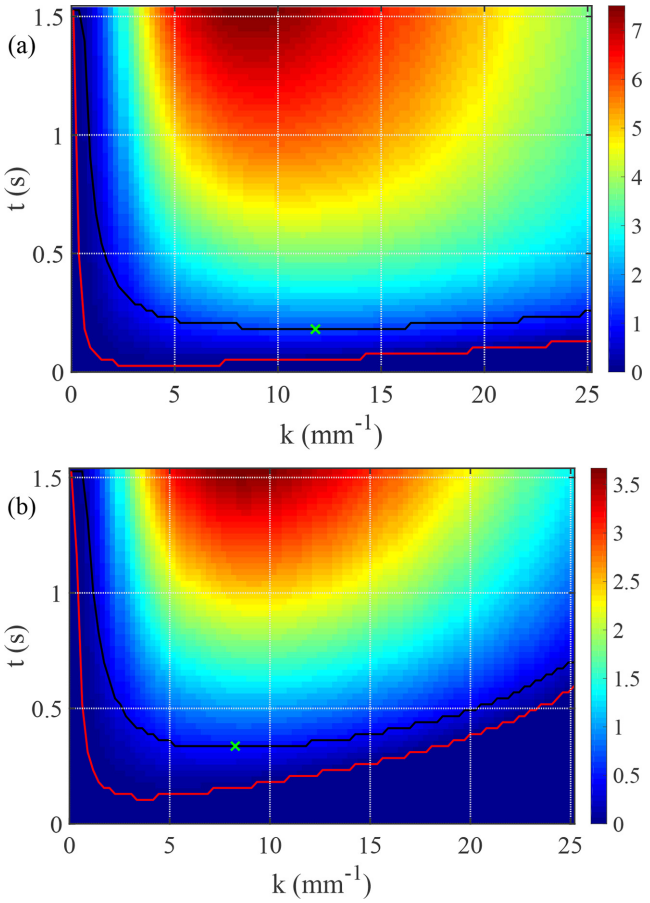

FIG. 2. Colormap of the growth rate σ (s^{-1}) of the instability as a function of time t and of the wavenumber k, for the first model (Sec. III A). Parameters are given into dimensional units (see Sec. III B for the parameters). Red line, a marginal instability threshold, $\sigma = 0$ (below this red line $\sigma < 0$). Black line, a threshold given by the *modified instability criterion*. Green cross, the onset position. Hundred values of k and 60 values of t are successively tested generating the displayed image. (a) Fast dissolution kinetics, $c_b = c_{b,S}$. (b) Slow dissolution kinetics with $\alpha = 3.63 \times 10^{-6}$ m s^{-1}, $c_b = c_{b,C}$. The slower dissolution velocity decreases the growth rate of the instability and delays the convection onset.

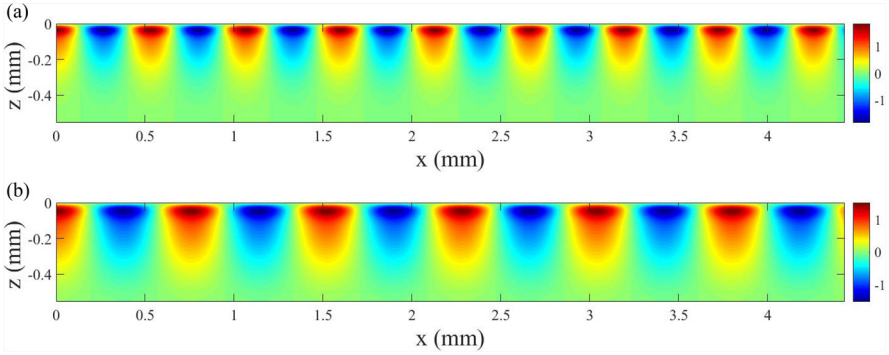

FIG. 3. Shape of the most unstable modes for the perturbed concentration field $c'(x,z)$ at the onset time with the modified criterion. Vertical system size $H_z = 0.55$ mm. (a) Fast dissolution kinetics, $c_b = c_{b,S}$. Wavelength 0.53 mm. (b) Slow dissolution kinetics with $\alpha = 3.63 \times 10^{-6}$ m s^{-1}, $c_b = c_{b,C}$. Wavelength 0.76 mm.

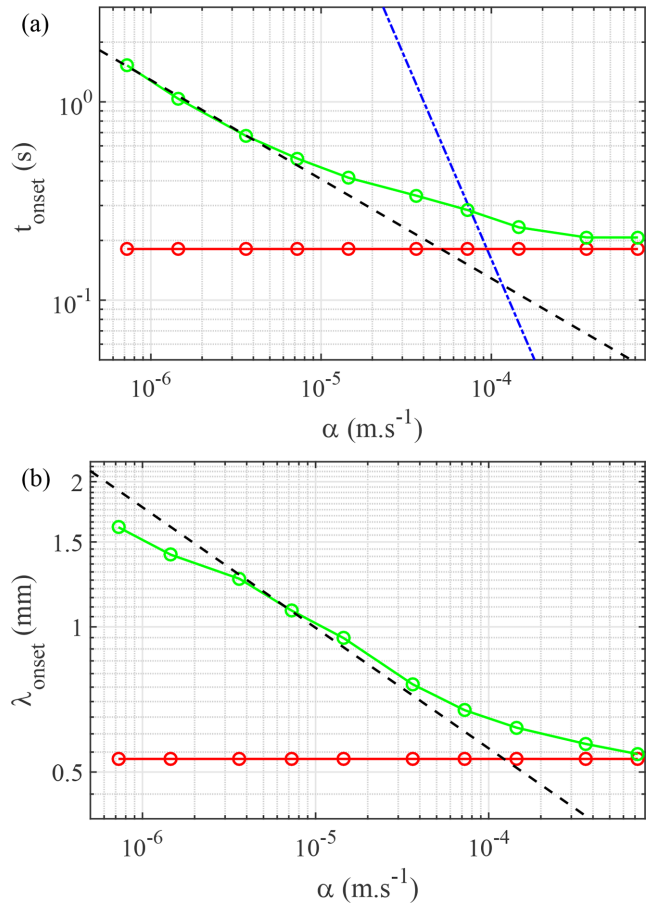

FIG. 4. Onset parameters onset time t_{onset} (a) and onset wavelength $\lambda = 2\pi/k_{onset}$ (b) as a function of α for a vertical size of $H_z = 50\,H$. Red curve, a modified instability criterion for $c_b = c_{b,S}$. Green curve, a modified instability criterion given for $c_b = c_{b,C}$. Dashed lines, scaling laws for $D_a \ll 1$, $t_{onset} \approx 1.4\sqrt{\nu/(\alpha\beta g)}$ and $\lambda_{onset} \approx 46\,(D^2\,\nu/(\alpha\beta g))^{1/4}$ [see Eqs. (12) and (11)]. As expected, the results are independent of α for $c_b = c_{b,S}$. We note for the range of α explored significantly longer onset times and larger onset wavelengths in the slow dissolution kinetics regime. We note significant differences between the cases $c_b = c_{b,S}$ and $c_b = c_{b,C}$ for $\alpha < 10^{-4}$. In this range with the modified instability criterion, the proposed scaling at small α is reasonable for t_{onset} and for λ_{onset}. For (a) only, dashed-dotted blue line, characteristic dissolution time D/α^2. The transition between fast and slow dissolution regimes for the onset prediction occurs when $t_{onset} \gtrsim D/\alpha^2$.

regime, t_{onset} and λ_{onset} become independent of α. We emphasize that the scaling laws at large D_a [Eqs. (8)–(10)] are by construction verified if the onset parameters do not depend on α or $\mathscr{H}$. The choice of the length L has been made such as $Ra = 1$ in the dimensionless system of equations, which implies these scaling laws by returning into physical units.

Finally, we investigate the behavior with the system size H_z, by varying the value of $\mathscr{H}$, but only in the case of fast dissolution kinetics ($c_b = c_{b,S}$), in order to keep a reasonable computational time. In Fig. 5, the results are found to not depend on H_z only for the modified instability criterion, which supports its use and shows the non-validity of the marginal instability criterion. The onset times appear indeed too short and the onset wavelengths too large with the marginal instability criterion. An onset wavelength growing with the system size appears also nonphysical. Experimentally for fresh water and salt, the wavelength is indeed of the order of a millimeter for a distance to the bottom of the tank very large (~ 10 cm) in front of the block size. With the *modified instability criterion*, we find that t_{onset} and λ_{onset} do not depend on H_z for $H_z > 0.4$ mm. With this dimensionalization corresponding to the salt parameters, we find $t_{onset} = 0.176$ s and $\lambda_{onset} = 0.529$ mm. However, the onset time is smaller than the values that we reported experimentally and numerically.[20] The prefactor of the scaling for $t_{onset} = K\,(\frac{\nu}{\beta g \sqrt{D}})^{2/3}$ is here $K = 2.30$, smaller by a factor 5.6 than the experimental value and by a factor 12.8 than the numerical value. This model thus provides the good order of magnitude but remains imprecise due to the strong hypotheses. The influence of the dissolution kinetics delays the onset instability. This discussion illustrates that the frozen base state assumption used with the marginal instability criterion is not valid for transient convection instabilities, when the fluid motion is described using the Navier–Stokes equations at large values of S_c. In contrast, the frozen base state assumption is commonly used to predict onset for the solutal convection in the porous media,[22,24,42] in which the Darcy equation replaces the Navier–Stokes ones.

IV. LINEAR STABILITY ANALYSIS: SECOND MODEL OF SECOND ORDER

A. Model

In Sec. III, we observe that using the marginal instability criterion, the wavelength of the fastest growing mode increases with the system size H_z [Fig. 5(b)]. One can think that this non-physical statement could be suppressed by incorporating the fluid acceleration in the linear instability. Foster[25] proposed a linear stability analysis

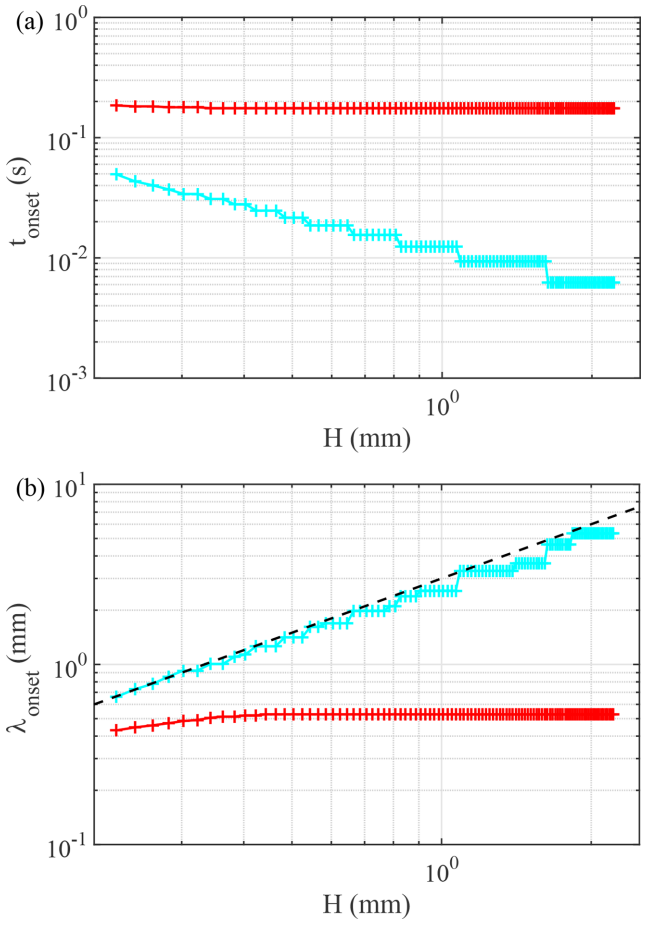

FIG. 5. Onset time t_{onset} (a) and onset wavelength $\lambda_{onset} = 2\pi/k_{onset}$ (b) as a function of H_z. Cyan curve, a marginal instability criterion for $c_b = c_{b,S}$. Red, a modified instability criterion for $c_b = c_{b,S}$. Black dashed curve, the line H_z vs H_z for (b) only. The marginal instability criterion provides too short times and too large wavelengths than expected. λ_{onset} is also growing with the system size H_z. The visible steps visible for the marginal instability criterion are due to the lack of resolution for the small values of k. With the modified criterion, the results are independent of the system size for $H_z > 0.4$ mm. For the salt parameters, we find $t_{onset} = 0.176$ s and $\lambda_{onset} = 0.529$ mm.

studying the transient thermal convection instability with a second order in time model incorporating the fluid acceleration term.

We start from the dimensionless system of linearized equations (15) and (16). By combining these two equations,[25] we eliminate the variable c' and obtain a single equation in w but with a second derivative in time, justifying the term of second order in time

$$\left(\frac{\partial}{\partial t} - \triangle\right)\left(\frac{1}{S_c}\frac{\partial}{\partial t} - \triangle\right)\triangle w = \triangle_1 w \frac{\partial c_b}{\partial z}. \tag{21}$$

Again, we consider the 2D domain O_{xz} (Fig. 1) of vertical extension $\mathscr{H}$ in dimensionless units. We seek a solution decomposed into horizontal normal modes of wavenumber k and into vertical Fourier modes under the form

$$w(x,z,t) = \int\left[\left(\sum_{m=1}^{\infty} A_m(t)\,\sin\left(m\pi z/\mathscr{H}\right)\right)\exp\left(i\,k\,x\right) + c.c.\right]\mathrm{d}k\,,$$

with $c.c.$ being the complex conjugate.

For given k and t, one obtains

$$\sum_{m=1}^{\infty}\left[\frac{1}{S_c}\left(-\frac{m^2\pi^2}{\mathscr{H}^2} - k^2\right)\ddot{A}_m(t)\,\sin\left(m\pi z/\mathscr{H}\right) - \left(1+\frac{1}{S_c}\right)\left(-\frac{m^2\pi^2}{\mathscr{H}^2} - k^2\right)^2 \dot{A}_m(t)\,\sin\left(m\pi z/\mathscr{H}\right) + \left(-\frac{m^2\pi^2}{\mathscr{H}^2} - k^2\right)^3 A_m(t)\,\sin\left(m\pi z/\mathscr{H}\right)\right] + k^2\frac{\partial c_b}{\partial z}\sum_{m=1}^{\infty} A_m(t)\,\sin\left(m\pi z/\mathscr{H}\right) = 0.$$

The term $\triangle_1 w\,\frac{\partial c_b}{\partial z}$ introduces non-diagonal terms, which are projected on the basis $A_m\,\sin\left(m\pi z/\mathscr{H}\right)$ by using the Galerkin method, i.e., by computing the integral of the previous equality multiplied by $\sin\left(r\pi z/\mathscr{H}\right)$ between $-\mathscr{H}$ and 0, with r an integer. We then get

$$\frac{1}{S_c}\left(-\frac{m^2\pi^2}{\mathscr{H}^2} - k^2\right)\ddot{A}_m(t) - \left(1+\frac{1}{S_c}\right)\left(-\frac{m^2\pi^2}{\mathscr{H}^2} - k^2\right)^2\dot{A}_m(t) + \left(-\frac{m^2\pi^2}{\mathscr{H}^2} - k^2\right)^3 A_m(t) + \frac{2k^2}{\mathscr{H}}\sum_{r=1}^{\infty} A_r(t)\,I_{rm}(t) = 0$$

with

$$I_{rm}(t) = \int_{-\mathscr{H}}^{0}\frac{\partial c_b}{\partial z}\sin\left(r\pi z/\mathscr{H}\right)\,\sin\left(m\pi z/\mathscr{H}\right)\mathrm{d}z\,.$$

To limit the computing time to manageable values, the integrals I_{rm} must be evaluated analytically, therefore, we restrict here our study to the case $c_b = c_{b,S}$ in the case of fast dissolution kinetics ($D_a \to \infty$). We suppose that the diffusive front $c_{b,S}$ does not reach the bottom of the system, i.e., the dimensionless time must roughly obey $t < \mathscr{H}^2/10$. With this hypothesis, the diffusive front can be approximated to the solution, for which the diffusive front is zero in $z = -H_z$. Foster[25] proposes in that case a simple analytic expression of $\sum_{r=1}^{\infty} A_r(t)\,I_{rm}(t)$, which is applied here. Then, we find by setting $B_m(t) = \dot{A}_m(t)$, the following differential system of order one in time:

$$\dot{B}_m(t) = -(S_c+1)\left(\frac{m^2\pi^2}{\mathscr{H}^2} + k^2\right)B_m(t) - S_c\left(\frac{m^2\pi^2}{\mathscr{H}^2} + k^2\right)^2 A_m(t) + \frac{k^2\,S_c}{\mathscr{H}\left(\frac{m^2\pi^2}{\mathscr{H}^2} + k^2\right)} \times \sum_{r=1}^{\infty} A_r(t)\left[\exp\left(-\left[\frac{(m-r)\pi}{\mathscr{H}}\right]^2 t\right) - \exp\left(-\left[\frac{(m+r)\pi}{\mathscr{H}}\right]^2 t\right)\right].$$

By doing a truncation at the order N, this differential system can be written under a matrix form, $\frac{\mathrm{d}V}{\mathrm{d}t} = M\,V$ with the vector

$V(t) = (A_1, \ldots, A_N, B_1, \ldots, B_N)^\top$ and the matrix M of size $2N \times 2N$, which is written by blocks

$$M = \begin{pmatrix} P_{mr} & Q_{mr} \\ R_{mr} & S_{mr} \end{pmatrix}.$$

We find the following coefficients:

$$\begin{aligned} P_{mr} &= 0, \\ Q_{mr} &= \delta_{mr}, \\ S_{mr} &= -(S_c+1)\left(\frac{m^2\pi^2}{\mathscr{H}^2}+k^2\right)\delta_{mr}, \text{ and} \\ R_{mr} &= -S_c\left(\frac{m^2\pi^2}{\mathscr{H}^2}+k^2\right)^2\delta_{mr} \\ &\quad + \frac{k^2\,S_c}{\mathscr{H}\left(\frac{m^2\pi^2}{\mathscr{H}^2}+k^2\right)}\left[e^{-\left[\frac{(m-r)\pi}{\mathscr{H}}\right]^2 t} - e^{-\left[\frac{(m+r)\pi}{\mathscr{H}}\right]^2 t}\right]. \end{aligned}$$

As done previously, we perform the linear stability analysis by computing, for given values of $\mathscr{H}$, k, and t, the eigenvalues of the matrix M. We seek the eigenvalue of largest real part σ. The marginal onset of instability is given when σ becomes positive for the shortest time, k being varied. The corresponding eigenvector provides the spatial shape of the most unstable mode. Again, we show in Sec. IV B that the criterion of marginal instability gives nonphysical results, with too short values of the onset times, because the frozen base state hypothesis is not valid for fluid convection. We adopt also the same *modified instability criterion*, $\sigma > \max_z\left(\frac{\partial c_{b,S}}{\partial t}\right) \approx \frac{e^{-1/2}}{\sqrt{2\pi}\,t} \approx \frac{0.24}{t}$.

B. Results

The linear stability analysis is always performed with MATLAB, and we use the same scale of correspondence between the computational and the dimensional physical space, corresponding to the parameters of dissolution of salt in fresh water. Again, the length scale H is chosen as $R_a = 1$, which gives for the parameters of salt ($\beta = 0.2$, $D = 1.61 \times 10^{-9}\,\mathrm{m^2\,s^{-1}}$, and $\nu = 1.66 \times 10^{-6}\,\mathrm{m^2\,s^{-1}}$),[19,20] $H \approx 1.11 \times 10^{-5}\,\mathrm{m}$. The timescale is then $H^2/D \approx 7.63 \times 10^{-2}\,\mathrm{s}$. The vertical size of the system is thus $H_z = \mathscr{H}\,H$.

By choosing N of the order of $\mathscr{H}$, we have a good convergence of the method. We start with a Schmidt number $S_c = 1000$ for the case of salt. In Fig. 6, we plot two colormaps of the values of σ as a function of k and t for two values of the system size H_z. The marginal instability criterion provides too short times of onset, whereas the modified criterion gives onset times of order 0.2 s. Compared with the results of the first model (Sec. III B) ($S_c \to \infty$), we note a weaker dependency of the onset with k and the onset time is slightly smaller. Moreover, larger wavenumbers appear more unstable than small wavenumbers, probably because the inertia of large-scale modes prevents them to grow fast.

The spatial shape of the most unstable velocity modes according to the modified criterion is plotted in Fig. 7 for $H_z = 0.55$ and $H_z = 2.22$ mm. Despite the difference of size between the two systems, the shape of these modes at the onset is very similar, with identical wavelength $\lambda_{onset} = 0.53$ mm. In the second case, the vertical extension of the velocity boundary layer is $\delta_v = 0.44$ mm, when defined as the distance between $z = 0$ and the further point where

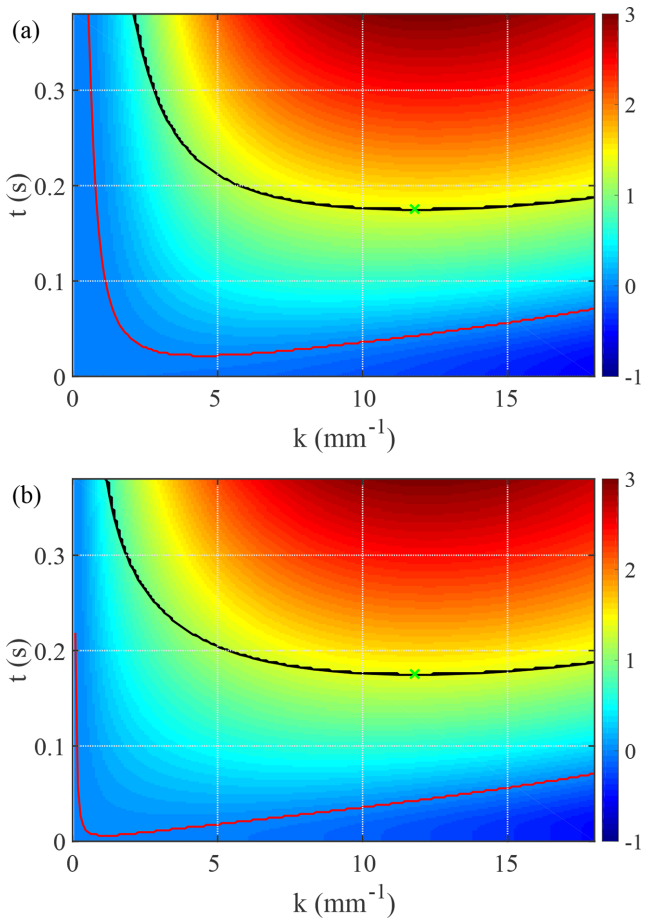

FIG. 6. Colormap of the growth rate σ ($\mathrm{s^{-1}}$) as a function of time t and of the wavenumber k for the second model (Sec. IV A). Red line, a marginal instability threshold, $\sigma = 0$ (below this red line $\sigma < 0$). Black line, a threshold given by the *modified instability criterion*. (a) σ in colormap as a function of k and of t for H = 50 or $H_z = 0.55$ mm. (b) The same H = 200 or $H_z = 2.22$ mm. In both cases, $S_c = 1000$.

$|w(z, x = \lambda/2)| < 0.1\max(|w(z, x = \lambda/2)|)$. With this definition, the ratio between the wavelength at onset and the size of the boundary layer $\lambda_{onset}/\delta_v = 1.20$ is lower than the ratio of 2.3 between the wavelength and the vertical system size for the classic Rayleigh–Bénard instability with a top solid surface and a bottom free surface.[40] However, in our case, the definition of the vertical boundary layer is arbitrary. The maximal vertical velocity in norm is located at the position $z = -0.11$ mm. The ratio of the wavelength by twice of this distance gives 2.5.

The dependency with the system size H_z is tested in Fig. 8 for $S_c = 1000$ and both instability criteria and two values of the number N, 100 and 200. We find for these values of N that the computation is reasonably converged for $H_z < 10$ mm corresponding to $\mathscr{H} < 1000$. Again, the marginal instability criterion gives nonphysical results with an onset wavelength, which grows with H_z. The fluid acceleration does not explain why the marginal instability criterion associated with the frozen base state assumption does not work for fluid convection,

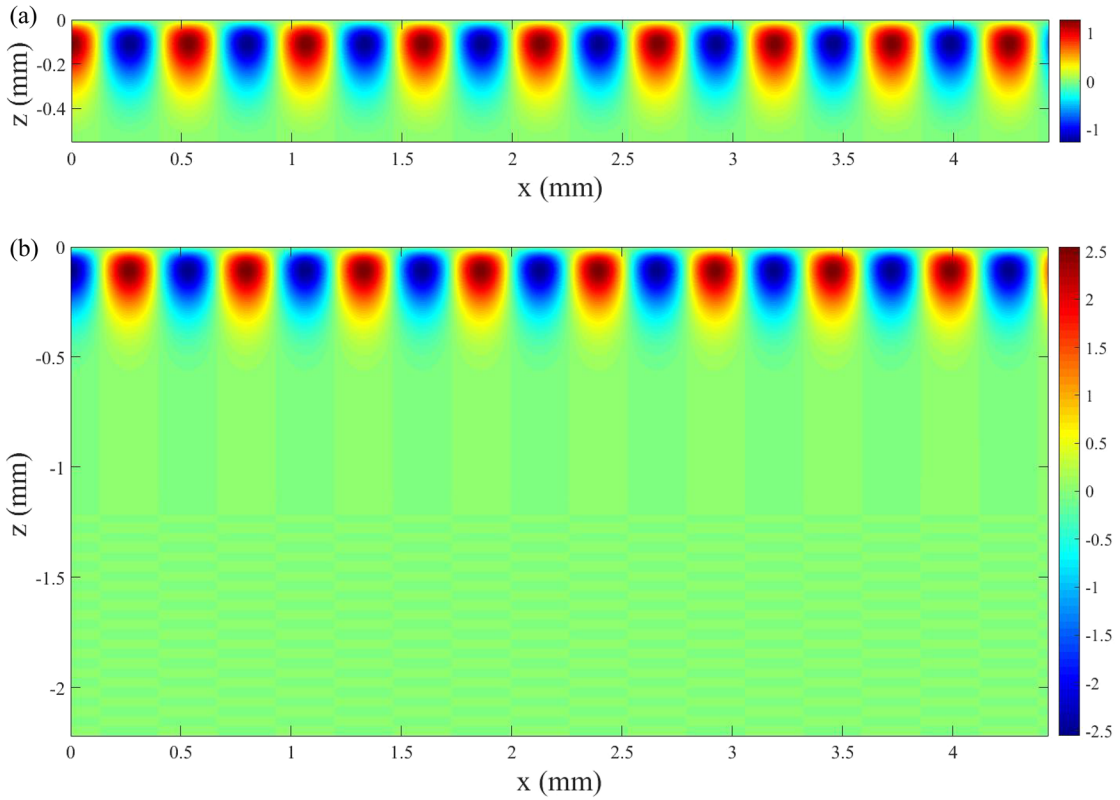

FIG. 7. Second model. (a) Shape of the most unstable modes for the perturbed vertical velocity field $w(x, z)$ at the onset time with the modified criterion. Top, H = 50 or $H_z = 0.55$ mm. (b) H = 200 or $H_z = 2.22$ mm. In both cases, the wavelength at the onset is equal to $\lambda_{onset} = 0.53$ mm, and the spatial shape of the modes is very similar despite the different aspect-ratio of the system. $S_c = 1000$.

contrary to the case of convection in the porous media. In contrast, using the modified instability criterion, we observe that the onset time and the onset wavelength are not depending on H_z, validating our approach to take into account the dynamics of the base state. However, rigorously a converged computation for growing values of H_z requires an increasing number of modes N to the detriment of the computing time. Nevertheless by extrapolating the results of the flat part of the curve to an infinite system, we find for salt that the convection would start at $t_{onset} = 0.176$ s with a wavelength $\lambda_{onset} = 0.531$ mm. These values for $S_c = 1000$ are nearly identical to those of the first model, validating the method. We obtain the proper order of magnitude, compared to the experimental measurements,[20] if we remember that the onset time is smaller than that of the time of plumes emission. However, the onset time measured in our numerical simulations (see Appendix C in Ref. 20) $t_{onset\ num} = 1.02$ s is larger than this last theoretical estimate and than that of the experimental estimation. By construction of the dimensionless system, the results of our stability analysis verify the scaling for the onset at large D_a [Eqs. (8)–(10)]. Then, one deduces a prefactor K for the onset time, $K = 2.31$, which is 12.8 times smaller than our numerical value and 5.54 times smaller than our experimental value.[20] Compared to the first model without the fluid acceleration, we find the same behavior, both models underestimate the onset times. This could be caused by an incorrect treatment of the velocity boundary conditions, as the non-slipping of the horizontal velocity is not imposed.

Finally, we test the influence of the value of S_c. In dimensionless units, we find that the t_{onset} and λ_{onset} are weakly depending on S_c, as we can see in Fig. 9. We observe a slight increase in t_{onset} when S_c is of order one. To express the results into dimensional units, we can choose to keep the diffusion coefficient constant, whereas the viscosity is varying. This approach is not physically justified, because these two quantities are often linked, for example, by the Stokes–Einstein relation for diffusion of solute in a liquid. A Schmidt number of order one occurs for a gas phase, like for diffusion of water vapor into air, where $D = 2.42 \times 10^{-5}$ m^2 s^{-1} (Ref. 39) at 25 °C, whereas the kinematic viscosity of air is $\nu = 1.52 \times 10^{-5}$ m^2 s^{-1} at the same temperature. This case is relevant to study the sublimation of ice into air.[19] Therefore, in Fig. 10, we plot the dependency of t_{onset} and λ_{onset} as a function of the S_c for a fixed kinematic viscosity $\nu = 1.66 \times 10^{-6}$ m^2 s^{-1} and for a variable diffusion coefficient $D = \nu/S_c$. With this choice, we find that t_{onset} increases and λ_{onset} decreases with S_c. However, performing the computation for a constant value of $\mathscr{H}$ implies in physical dimensional units, a varying system size $H_z = \mathscr{H} H$, because H is defined as the scale for which $R_a = 1$. Finally, we note that the choice of D constant and ν variable gives an increase in λ_{onset} with S_c according to the scaling Eq. (9) and in agreement with our numerical simulations.[20]

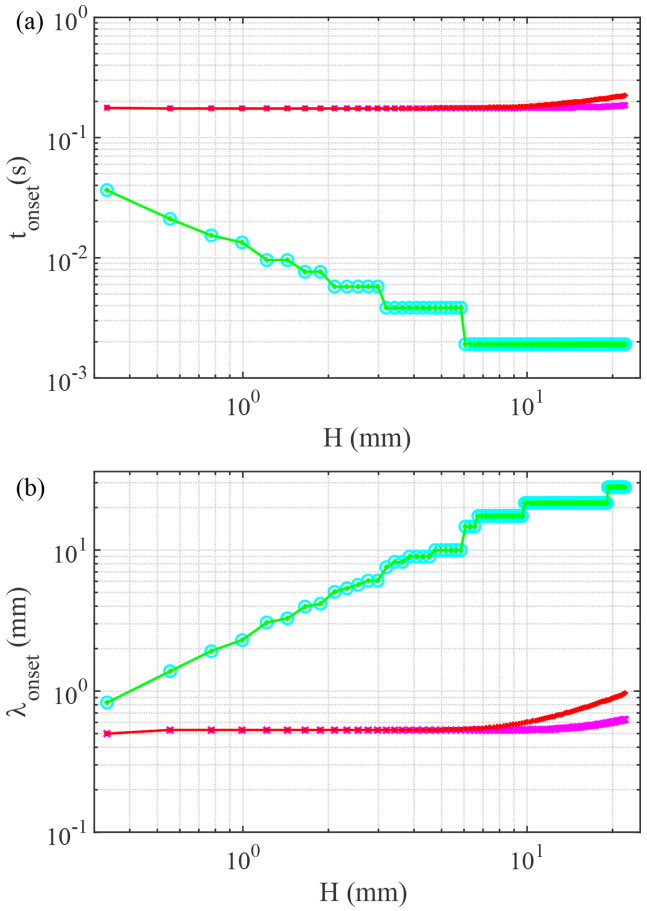

FIG. 8. Second model. Onset time t_{onset} (a) and onset wavelength $\lambda_{onset} = 2\pi/k_{onset}$ (b) as a function of H_z for $Sc = 1000$. Comparison between the marginal instability criterion (green for $N = 100$ and cyan $N = 200$) and the modified instability criterion (red $N = 100$ and magenta $N = 200$). At low enough H_z and sufficient value of N, the results with the modified criterion are independent of H_z, validating the approach. The results are identical for both values of N when $H_z < 5$ mm and differ notably when $H_z > 10$ mm, the flat behavior being extended with $N = 200$. We find $t_{onset} = 0.176$ s and $\lambda_{onset} = 0.531$ mm (salt parameters).

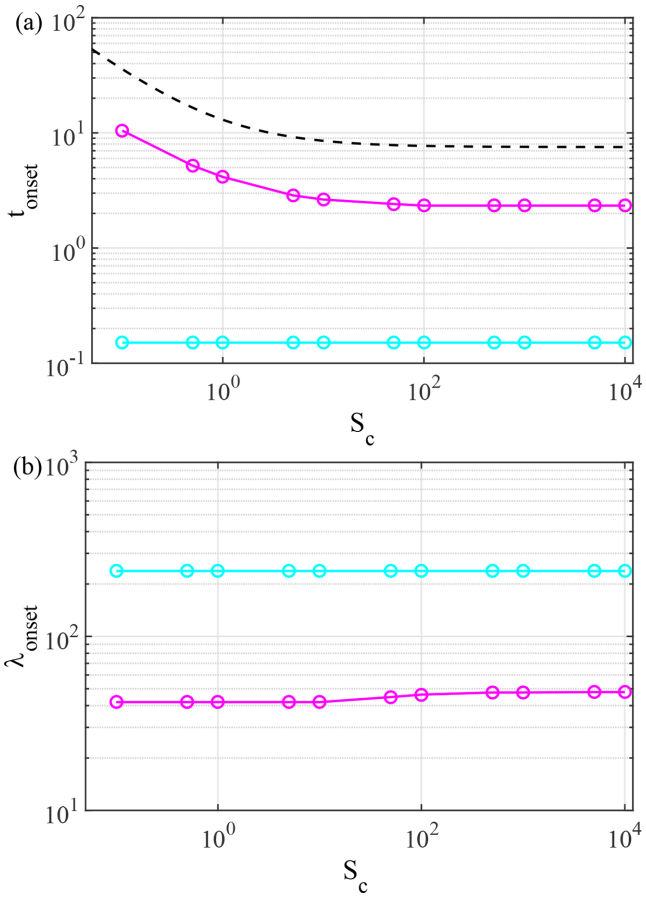

FIG. 9. Second model. Onset time t_{onset} (a) and onset wavelength $\lambda_{onset} = 2\pi/k_{onset}$ (b) as a function of S_c, for $\mathscr{H} = 100$. Comparison between the marginal instability criterion (cyan $N = 100$) and the modified instability criterion (magenta $N = 100$). We observe a weak dependency of onset parameters with S_c. Black dashed line for the left panel, prediction of t_{onset} according to the propagation theory Eq. (22).

V. DISCUSSION

We have performed a linear stability analysis of solutal convection, occurring when a soluble body is suddenly put in a contact with a fluid. Due to the strong hypotheses made, the results of this linear stability analysis remain qualitative. Nevertheless, we can draw several interesting points. Our method translates the linearized partial differential equations obeyed by the perturbations [Eqs. (17) and (18)] into a linear ordinary differential system of coupled spatial modes using a Fourier series decomposition. The marginal criterion of instability is given for the largest eigenvalue by the first positive value in time. This eigenvalue corresponds to the temporal growth rate of the most unstable perturbation. We note that one may prefer to integrate numerically the linear system as a function of time[25] and to define the onset when perturbation has been amplified by a given factor. However, with this amplification method, the onset parameters are found to depend notably on the initial conditions and several noise realizations are thus required.[25,47] Then, by computing the eigenvalues, we find that contrary to the convection in the porous media, assuming the base state frozen, the marginal instability criterion gives non-physical results, with too short t_{onset} and too large λ_{onset}. The difference consists in a different structure of the viscous friction term: proportional to the pressure gradient for the Darcy equation and proportional to the Laplacian of the velocity field for the Navier–Stokes equations. In the porous media, viscous dissipation occurs at the pore scale, which is supposed small compared to all the scales involved in the instability, and all wavelengths are equivalently damped. The problem is also weakly dependent on boundary conditions. In contrast, with the viscous Laplacian term of the Navier–Stokes equations, large scale structures are less damped and modes with a size comparable to the system size become unstable according to the marginal instability criterion. The failure of this hypothesis had been already reported in the seventies.[47] Qualitatively, the failure of this criterion could be explained by considering the time domain between t_{onset} given by the marginal

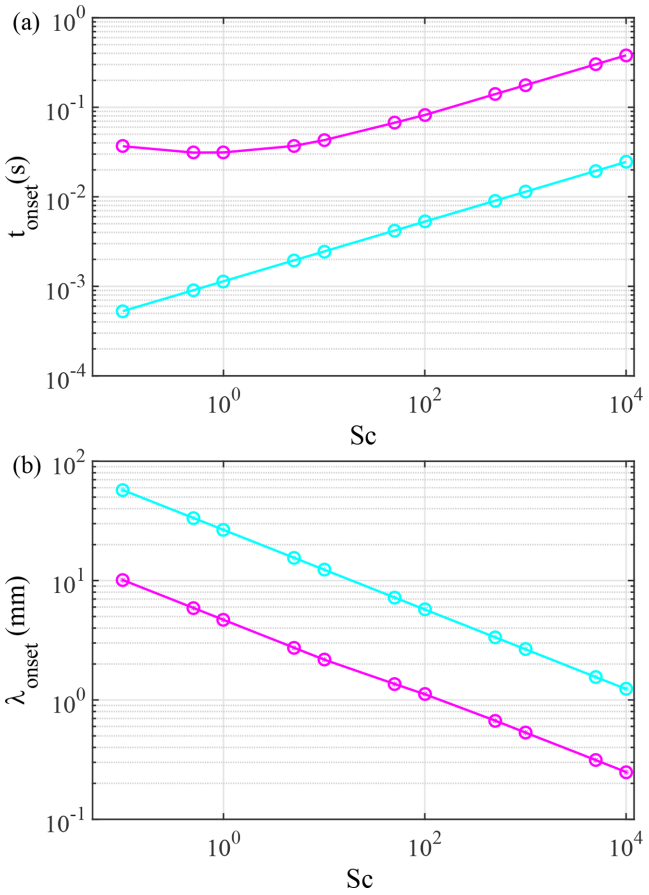

FIG. 10. Second model. Onset time t_{onset} (a) and onset wavelength $\lambda_{onset} = 2\pi/k_{onset}$ (b) as a function of S_c for fixed $\nu = 1.66 \times 10^{-6}$ m^2 s^{-1} and $D = \nu/S_c$ in dimensional units for H = 100 (varying values of H_z). Comparison between the marginal instability criterion (cyan $N = 100$) and the modified instability criterion (magenta $N = 100$).

instability and the larger t_{onset} corresponding to the experimental observations. In this domain, the concentration and velocity perturbations are unstable, but their growths are slower than the base state temporal evolution and these perturbations are not detectable. This idea motivates the definition of the modified instability criterion, which supposes that the growth rate of perturbation must be larger than the rate of change of the base state. In fact, this criterion provides a qualitative physic interpretation of the onset, which does not appear clearly in the numerical simulations.

Using this modified criterion, we observe also in our results a weak selectivity into the wave number due to the flatness of the instability curve plotted as a function of k. Consequently, the experimental wavelength could not be well defined and very sensitive to the surrounding noise. Then using the first model, we investigate the effect of the dissolution kinetics through the coefficient α, which changes the shape of the base state. We observe a delay of the appearance of convection and a slight change of the associated wavelength. The results of our analysis are in agreement with the scaling derived for slow dissolution kinetics ($D_a \ll 1$), when α is varied as illustrated in Fig. 4.

With the second model, the dependency with the Schmidt number S_c expressed in dimensionless units is weak for the onset parameters. Finally, the comparison with the experiments and the numerical simulations performed for the dissolution of salt in water (see Ref. 20) show that we obtain the correct orders of magnitude, but underestimating the coefficient K for the onset [Eq. (10)] by a factor 5.6 (the first model, $S_c \gg 1$) and by a factor 5.5 (the second model, $S_c = 1000$). The difference with the numerical simulations[20] is larger with a factor 12.8 for both models. This larger difference between the numerical simulations and the linear instability than with the experiments is surprising, because all the hypotheses in the numerical simulations are also used for the linear stability analysis. Nonlinear terms are incorporated in the simulations, and the onset time is defined by detecting the appearance of a transverse structure in the concentration field. In experiments, we cannot exclude also a systematic bias in the visual determination of the onset time. We also note that the two models give the same orders of magnitude, but the values for t_{onset} at a large Schmidt number ($S_c = 1000$ in the second model) differ by a factor 2.5. The first model describes the instability of the perturbation concentration field c', whereas the second addresses the instability of the vertical velocity field w. However, as these two fields are coupled, the analysis must be equivalent. This discrepancy could be caused by a significant effect of the acceleration term even for $S_c = 1000$. Moreover, the modified criterion is not really justified mathematically and thus should not be used to predict precise values. The pragmatic approach of Tan and Thorpe[35] for fixed temperature at the boundaries can also be applied to our problem for fast dissolving kinetics, when the concentration is fixed at the top boundary and $c(z = 0) = c_{sat}$. For a top solid surface and a bottom free surface and the fixed temperature or concentration, the critical Rayleigh number is $Ra_c = 1100.7$. Then the onset time is $t_{onset} = K\left(\frac{\nu}{\beta g \sqrt{D}}\right)^{2/3}$, with $K = 37.0$. Compared to experiments and numerical simulations, this value is better than the simple estimate $K = 106.6$ and closer to our experimental $K \approx 12.8$ and numerical $K \approx 29.5$ estimates in Ref. 20.

Several critics can be addressed to our theoretical study. First, the proper boundary conditions for the velocity field are not implemented, which can modify significantly the values of onset parameters. Using the decomposition in a base of orthonormal functions[26] adapted for a semi-infinite system like the Chebyshev polynomials[48] instead of the decomposition into the Fourier series could solve this problem and reduce the computational time. The semi-infinite geometry would also be more appropriate to describe the experiments, where the tank depth is large compared to the size of the dissolving block. We expect to obtain qualitatively similar results but with different prefactor values. Moreover, the modified instability criterion, needed to take into account the evolution of the base state is not justified theoretically, although it gives the good orders of magnitude. Comparable results are provided by the propagation theory, where the solid boundary conditions are used for the velocity field and where a part of the dynamic of the base state is taken into account.[28–30] For a given wavenumber, a self-similar change of variable adapted to the diffusing base state transforms the space–time problem to the study of the stability of two coupled ordinary differential equations. A base state, taking into account the dissolution kinetics by the coefficient α thus cannot be tested with this method, as the solution Eq. (4) is not self-similar. Moreover, we note that an assumption equivalent to our modified instability criterion is done supposing the equality between the growth

rate of the perturbation and the one of the base states. From a numerical exploration of parameters,[49] the following evolution for the onset time is obtained in dimensional units:

$$t_{onset} = 7.53 \left[1 + \left(\frac{0.804}{S_c}\right)^{3/4}\right]^{8/9} \left(\frac{\nu}{\beta g \sqrt{D}}\right)^{2/3}. \quad (22)$$

For salt, $S_c \approx 1000$, the term with the Schmidt number is negligible and the prefactor prediction for the onset time becomes $K = 7.53$. The curve becomes closer to the experimental points[20] and differs by a factor 1.7. The corresponding wavenumber of the convection instability at the onset is given by the scaling $k_{onset} = 0.53/\left(\sqrt{D}\, t_{onset}\right)$.[49] For salt, we obtain then $\lambda_{onset} = 7.62 \times 10^{-4}$ m, which is compatible with the order of magnitude of the first wavelength observed in dissolution patterns.[19] Compared to our linear stability analysis (the second model), the propagation theory predicts onset times three times larger, but the trends with the Schmidt number are similar to we can see in Fig. 9 (left).

In addition, the domain of validity of the linear analysis may be small. In experiments and in numerical simulations, the nonlinear interactions between modes at different wavenumbers play likely a role in the emission of convective plumes, especially because this analysis suggests a weak selection in k of the fastest growing mode (see Figs. 2 and 6). We also note, than in reality, the instability occurs in a three-dimensional space and the width of the dissolving block is most of the time smaller than the width of the liquid bath, which may induce finite size effects. Therefore, the comparison of the onset parameters between experiments with numerical simulations and results from a linear stability analysis remains difficult.

From a theoretical point of view, a linear stability analysis valid for infinitesimal perturbations is also a necessary condition but not sufficient, because a transient growth of a mode could be interpreted as the onset of the convection. The study must be completed by an energy stability analysis keeping nonlinear terms, which guarantees that finite perturbations decay exponentially in the domain of the stability.[31,42] In our case, the previous numerical simulations[20] and experiments[19] show that the found onset is not a transient growth and is even followed by a quasi-stationary regime. The determination of the onset of an instability when the base state is depending on time thus remains theoretically a difficult question. The most rigorous approach, the non-normal linear stability analysis[32–34] requires us to perform numerical simulations of the adjoint problem to find the optimal perturbations. However, the determined onset parameters by this last method are only found in qualitative agreement with the experiments.[33] The recent linear optimal transient growth method was recently proposed to address the Rayleigh–Taylor instability in the presence of a varying thickness of the fluid layer due to a flow.[50,51] This method could also be adapted for transient fluid convection. We also note that few experimental works determine carefully the onset for instabilities with a unsteady base state, for example, the buoyancy-driven instability in the presence of a radial injection.[52] Therefore, decisive confrontations between theories and experiments remain missing for these kinds of hydrodynamic instabilities, whose the solutal convection induced by dissolution constitutes a practical and relevant case. Further theoretical work in combination with numerical simulations is thus required. In geomorphology, a theoretical prediction of the onset of solutal convection is important for the growth of cavities filled with quescient water by dissolution, in particular, for the water dissolution of gypsum.[10,53]

ACKNOWLEDGMENTS

Julien Philippi acknowledges a postdoctoral grant from CNRS at MSC. This research was partially funded by the ANR Grant Erodiss No. ANR-16-CE30-0005. We thank Maurice Rossi, Benjamin Miquel, and Laurent Limat for scientific discussions. We are grateful to the anonymous reviewers for their constructive comments, which helped us to improve this work.

APPENDIX: DERIVATION OF THE MATRIX COEFFICIENTS USED IN SECTION III A

We detail here the derivation of the matrix coefficients B_{mn}, C_{mn}, D_{mn}, and E_{mn} involved in the first model valid for large Sc, using the Galerkin method. We consider the linear differential system Eqs. (17) and (18), where the temporal derivative is neglected in the second equation in the limit $S_c \gg 1$. We look for solutions of $\tilde{c}$ and $\tilde{w}$ under the form of a Fourier series in z truncated to order N

$$\tilde{c}(z,t) = \sum_{n=1}^{N} \gamma_n(t)\, \theta_n(z), \quad (A1)$$

$$\tilde{w} = \sum_{n=1}^{N} w_n(t)\, \chi_n(z). \quad (A2)$$

Here, $\theta_n(z)$ and $\chi_n(z)$ are the base functions verifying the boundary conditions

$$\theta_n(z) = \sin\left(\frac{2n-1}{2}\frac{\pi}{R}z\right), \quad (A3)$$

$$\chi_n(z) = \sin\left(\frac{2n}{2}\frac{\pi}{R}z\right). \quad (A4)$$

Equation (17) is multiplied by $\theta_m(z)$ and Eq. (18) by $\chi_m(z)$, and we integrate with respect to z between $-\mathscr{H}$ and 0

$$\int_{-\mathscr{H}}^{0} \frac{\partial \tilde{c}}{\partial t}\theta_m \,\mathrm{d}z = -\int_{-\mathscr{H}}^{0} \tilde{w}\frac{\partial c_b}{\partial z}\theta_m \,\mathrm{d}z + \int_{-\mathscr{H}}^{0} \frac{\partial^2 \tilde{c}}{\partial z^2}\theta_m \,\mathrm{d}z - \int_{-\mathscr{H}}^{0} k^2 \tilde{c}\,\theta_m \,\mathrm{d}z$$

and

$$\int_{-\mathscr{H}}^{0} k^4\, \tilde{w}\, \chi_m \,\mathrm{d}z + \int_{-\mathscr{H}}^{0} \frac{\partial^4 \tilde{w}}{\partial z^4}\, \chi_m \,\mathrm{d}z - \int_{-\mathscr{H}}^{0} 2k^2\, \frac{\partial^2 \tilde{w}}{\partial z^2}\, \chi_m \,\mathrm{d}z + \int_{-\mathscr{H}}^{0} k^2\, \tilde{c}\, \chi_m \,\mathrm{d}z = 0 .$$

We express these equations as sums of index N to obtain the m line of a matrix product. One gets

$$\begin{aligned}\sum_{n=1}^{N} \frac{\partial}{\partial t}\gamma_n(t) \int_{-\mathscr{H}}^{0} \theta_n(z)\,\theta_m(z)\mathrm{d}z &= -\sum_{n=1}^{N} w_n(t) \int_{-\mathscr{H}}^{0} \chi_n\,\theta_m\,\frac{\partial c_b}{\partial z}\mathrm{d}z \\ &+ \sum_{n=1}^{N} \gamma_n(t) \int_{-\mathscr{H}}^{0} \frac{\partial^2 \theta_n(z)}{\partial z^2}\,\theta_m(z)\,\mathrm{d}z \\ &- \sum_{n=1}^{N} k^2 \gamma_n(t) \int_{-\mathscr{H}}^{0} \theta_n(z)\,\theta_m(z)\,\mathrm{d}z \end{aligned} \quad (A5)$$

and

$$\sum_{n=1}^{N} w_n(t)\, k^4 \int_{-\mathscr{H}}^{0} \chi_n(z)\, \chi_m(z)\, \mathrm{d}z + \sum_{n=1}^{N} w_n(t) \left(\frac{n\pi}{\mathscr{H}}\right)^4 \int_{-\mathscr{H}}^{0} \chi_n(z)\, \chi_m(z)\, \mathrm{d}z + \sum_{n=1}^{N} w_n(t)\, 2k^2 \left(\frac{n\pi}{\mathscr{H}}\right)^2 \int_{-\mathscr{H}}^{0} \chi_n\, \chi_m\, \mathrm{d}z + \sum_{n=1}^{N} \gamma_n(t)\, k^2 \int_{-\mathscr{H}}^{0} \theta_n(z)\, \chi_m(z) \mathrm{d}z = 0. \quad \text{(A6)}$$

These expressions involve several integrals, which must be calculated now. With the orthogonality of the base functions, one obtains first

$$\int_{-\mathscr{H}}^{0} \theta_n(z)\, \theta_m(z) \mathrm{d}z = \frac{\mathscr{H}}{2} \delta_{mn},$$
$$\int_{-\mathscr{H}}^{0} \chi_n(z)\, \chi_m(z) \mathrm{d}z = \frac{\mathscr{H}}{2} \delta_{mn}.$$

The cross term between θ_n and χ_n induces non-diagonal contributions [last line of Eq. (A6)]

$$\begin{aligned} Q_{mn} &= \int_{-\mathscr{H}}^{0} \theta_n\, \chi_m \mathrm{d}z \\ &= \int_{-\mathscr{H}}^{0} \sin\left(\frac{2n-1}{2}\frac{\pi}{\mathscr{H}} z\right) \sin\left(m\frac{\pi}{\mathscr{H}} z\right) \mathrm{d}z \\ &= \frac{4m}{4m^2-(2n-1)^2} \frac{\mathscr{H}}{\pi} (-1)^{m+n} \\ &= (1/k^2) \times D_{mn} \times \mathscr{H}. \end{aligned}$$

The most complex term corresponds to the projection of the base state gradient $\partial c_b/\partial z$ [the second line of Eq. (A5)].

$$P_{mn} = \int_{-\mathscr{H}}^{0} \chi_n\, \theta_m\, \frac{\partial c_b}{\partial z} \mathrm{d}z.$$

In most cases, this term must be computed numerically to obtain the matrix terms. However, in the limit $Da \ll 1$, the expression of the base state under a Fourier series $c_{b,S}$ [Eq. (14)] can be used, which is very close to the solution $c_{b,E} = \mathrm{erfc}(z/(2\sqrt{t}))$ at short times. Then, an analytic solution can be found

$$P_{mn} = \int_{-\mathscr{H}}^{0} \left[\sin\left(\frac{n\pi}{\mathscr{H}} z\right) \sin\left(\frac{2m-1}{2}\frac{\pi}{\mathscr{H}} z\right) \times \sum_{p=1}^{\infty} \frac{2}{\mathscr{H}} e^{-\left((2p-1)\frac{\pi}{2\mathscr{H}}\right)^2 t} \cos\left(\frac{2p-1}{2\mathscr{H}} \pi z\right) \mathrm{d}z \right].$$

Using trigonometry relations, one finds

$$P_{mn} = \frac{1}{2} \left(e^{-\left((2(m-n)-1)\frac{\pi}{2\mathscr{H}}\right)^2 t} - e^{-\left((2(n+m)-1)\frac{\pi}{2\mathscr{H}}\right)^2 t} \right).$$

The differential system [Eqs. (A5) and (A6)] can now be written under a matrix form using the vectors $V = (\gamma_1, \ldots, \gamma_N)^\top$ and $W = (w_1, \ldots, w_N)^\top$. These equations become

$$\frac{\mathscr{H}}{2} \frac{\mathrm{d}V}{\mathrm{d}t} = -P\, W - \left(\frac{\pi}{\mathscr{H}} \frac{2n-1}{2}\right)^2 \frac{\mathscr{H}}{2}\, V - k^2 \frac{\mathscr{H}}{2}\, V,$$

and the second

$$W \left(k^4 \frac{\mathscr{H}}{2} + \left(\frac{n\pi}{\mathscr{H}}\right)^4 \frac{\mathscr{H}}{2} + 2k^2 \left(\frac{n\pi}{\mathscr{H}}\right)^2 \frac{\mathscr{H}}{2} \right) = -\mathscr{H}\, D\, V.$$

Defining the matrix

$$E_{mn} = \frac{1}{2} \left[k^4 + \left(\frac{n\pi}{\mathscr{H}}\right)^4 + 2k^2 \left(\frac{n\pi}{\mathscr{H}}\right)^2 \right] \delta_{mn},$$

with I being the identity matrix, one obtains $W = E^{-1} D\, V$. Reporting this expression in the time evolution of V, one gets with $C = -2P/(\mathscr{H})$

$$\frac{\mathrm{d}V}{\mathrm{d}t} = -C E^{-1} D\, V + \left[-\frac{k^2}{2} - \left(\frac{\pi}{\mathscr{H}} \frac{2n-1}{2}\right)^2 \right] V.$$

Finally, the differential system reads $\frac{dV}{dt} = A(t)\, V$ with $A = B - C E^{-1} D$, where

$$\begin{aligned} B_{mn} &= -\left[k^2 + \left(\frac{(2n-1)\pi}{2\mathscr{H}}\right)^2 \right] \delta_{mn}, \\ C_{mn} &= \frac{1}{\mathscr{H}} \left[\exp(-[(m+n-1/2)\pi/\mathscr{H}]^2\, t) - \exp(-[(m-n-1/2)\pi/\mathscr{H}]^2\, t) \right], \\ D_{mn} &= \frac{k^2}{\pi} (-1)^{m+n} \frac{4m}{4m^2-(2n-1)^2}, \\ E_{mn} &= \frac{1}{2} \left[k^4 + \left(\frac{n\pi}{\mathscr{H}}\right)^4 + 2k^2 \left(\frac{n\pi}{\mathscr{H}}\right)^2 \right] \delta_{mn}. \end{aligned}$$

In the case $c_b = c_{b,S}$ (fast dissolution kinetics), we find the exact matrix coefficients given in Sec. III A.

DATA AVAILABILITY

The data that support the findings of this study are available from the corresponding author upon reasonable request.

REFERENCES

[1] K. H. Kang, H. C. Lim, H. W. Lee, and S. J. Lee, "Evaporation-induced saline Rayleigh convection inside a colloidal droplet," Phys. Fluids **25**, 042001 (2013).

[2] J. Dunstan, K. J. Lee, S. F. Park, Y. Hwang, and R. E. Goldstein, "Evaporation-driven convective flows in suspensions of non-motile bacteria," Phys. Rev. Fluids **3**, 123102 (2018).

[3] S. Tait and C. Jaupart, "Compositional convection in viscous melts," Nature **338**, 571–574 (1989).

[4] S. Tait and C. Jaupart, "Compositional convection in viscous melts," J. Geophys. Res. **97**, 6735–6756, https://doi.org/10.1029/92JB00016 (1992).

[5] R. C. Kerr, "Convective crystal dissolution," Contrib. Mineral. Petrol. **121**, 237–246 (1995).

[6] D. Gechter, P. Huggenberger, P. Ackerer, and H. N. Waber, "Genesis and shape of natural solution cavities within salt deposits," Water Resour. Res. **44**, W11409, https://doi.org/10.1029/2007WR006753 (2008).

[7] C. Oltean, F. Golfier, and M. Bués, "Numerical and experimental investigation of buoyancy-driven dissolution in vertical fracture," J. Geophys. Res. **118**, 2038, https://doi.org/10.1002/jgrb.50188 (2013).

[8]S. Kempe, "Cave genesis in gypsum with particular reference to underwater conditions," Cave Sci. J. Br. Speleol. Assoc. **49**, 1–6 (1972), available at https://www.researchgate.net/publication/232815431.
[9]S. Kempe, "Gypsum karst of Germany," Int. J. Speleol. **25**, 209–224 (1996).
[10]H. Luo, F. Laouafa, G. Debenest, and M. Quintard, "Large scale cavity dissolution: From the physical problem to its numerical solution," Eur. J. Mech. B **52**, 131–146 (2015).
[11]A. B. Klimchouk, *Hypogene Speleogenesis: Hydrogeological and Morphogenetic Perspective* (National Cave and Karst Research Institute, Carlsbad, NM, 2007).
[12]J. A. Neufeld, M. A. Hesse, A. Riaz, M. A. Hallworth, H. A. Tchelepi, and H. E. Huppert, "Convective dissolution of carbon dioxide in saline aquifers," Geophys. Res. Lett. **37**, L22404, https://doi.org//10.1029/2010GL044728 (2010).
[13]H. E. Huppert and J. A. Neufeld, "The fluid mechanics of carbon dioxide sequestration," Annu. Rev. Fluid Mech. **46**, 255–272 (2014).
[14]A. C. Slim, "Solutal-convection regimes in a two-dimensional porous medium," J. Fluid Mech. **741**, 461–491 (2014).
[15]J. Schürr, "Sur la vitesse de dissolution des sels dans leurs solutions aqueuses," J. de Phys. Théor. Appl. **4**, 17–26 (1905).
[16]T. S. Sullivan, Y. Liu, and R. E. Ecke, "Turbulent solutal convection and surface patterning in solid dissolution," Phys. Rev. E **54**, 486 (1996).
[17]C. Cohen, M. Berhanu, J. Derr, and S. Courrech du Pont, "Erosion patterns on dissolving and melting bodies (2015 gallery of fluid motion)," Phys. Rev. Fluids **1**, 050508 (2016).
[18]M. S. Davies Wykes, J. M. Huang, G. A. Hajjar, and L. Ristroph, "Self-sculpting of a dissolvable body due to gravitational convection," Phys. Rev. Fluids **3**, 043801 (2018).
[19]C. Cohen, M. Berhanu, J. Derr, and S. Courrech du Pont, "Buoyancy driven dissolution of inclined blocks: Erosion rate and pattern formation," Phys. Rev. Fluids **5**, 053802 (2020).
[20]J. Philippi, M. Berhanu, J. Derr, and S. Courrech du Pont, "Solutal convection induced by dissolution," Phys. Rev. Fluids **4**, 103801 (2019).
[21]I. G. Currie, "The effect of heating rate on the stability of stationary fluids," J. Fluid Mech. **29**, 337–347 (1967).
[22]J. Ennis-King, I. Preston, and L. Paterson, "Onset of convection in anisotropic porous media subject to a rapid change in boundary conditions," Phys. Fluids **17**, 084107 (2005).
[23]A. Riaz, M. A. Hesse, H. A. Tchelepi, and F. M. Orr, "Onset of convection in a gravitationally unstable diffusive boundary layer in porous media," J. Fluid Mech. **548**, 87–111 (2006).
[24]A. C. Slim and T. S. Ramakrishnan, "Onset and cessation of time-dependent, dissolution-driven convection in porous media," Phys. Fluids **22**, 124103 (2010).
[25]T. D. Foster, "Stability of a homogeneous fluid cooled uniformly from above," Phys. Fluids **8**, 1249 (1965).
[26]T. D. Foster, "Effect of boundary conditions on the onset of convection," Phys. Fluids **11**, 1257 (1968).
[27]M. Kaviany, "Onset of thermal convection in a fluid layer subjected to transient heating from below," J. Heat Transfer **106**, 817–823 (1984).
[28]C. K. Choi, J. H. Park, M. C. Kim, J. D. Lee, J. J. Kim, and E. J. Davis, "The onset of convective instability in a horizontal fluid layer subjected to a constant heat flux from below," Int. J. Heat Mass Transfer **47**, 4377–4384 (2004).
[29]C. F. Ihle and Y. Nino, "The onset of nonpenetrative convection in a suddenly cooled layer of fluid," Int. J. Heat Mass Transfer **49**, 1442–1451 (2006).
[30]M. C. Kim and S. G. Lee, "Onset of solutal convection in liquid phase epitaxy system," Korean J. Chem. Eng. **26**, 21–25 (2009).
[31]G. M. Homsy, "Global stability of time-dependent flows: Impulsively heated or cooled fluid layers," J. Fluid Mech. **60**, 129–139 (1973).
[32]F. Doumenc, T. Boeck, B. Guerrier, and M. Rossi, "Transient rayleigh-bénard-marangoni convection due to evaporation: A linear non-normal stability analysis," J. Fluid Mech. **648**, 521–539 (2010).
[33]T. Köllner, M. Rossi, F. Broer, and T. Boeck, "Chemical convection in the methylene-blue-glucose system: Optimal perturbations and three-dimensional simulations," Phys. Rev. E **90**, 053004 (2014).
[34]O. S. Kerr and Z. Gumm, "Thermal instability in a time-dependent base state due to sudden heating," J. Fluid Mech. **825**, 1002–1034 (2017).
[35]K. K. Tan and R. B. Thorpe, "The onset of convection driven by buoyancy effects caused by various modes of transient heat conduction: Part I. Transient Rayleigh numbers," Chem. Eng. Sci. **54**, 225–238 (1999).
[36]P. Meakin and B. Jamtveit, "Geological pattern formation by growth and dissolution in aqueous systems," Proc. R. Soc. A **466**, 659 (2010).
[37]J. Crank, *The Mathematics of Diffusion* (Clarendon Press, Oxford, 1975).
[38]M. Alkattan, E. H. Oelkers, J.-L. Dandurand, and J. Schott, "Experimental studies of halite dissolution kinetics, 1 the effect of saturation state and the presence of trace metals," Chem. Geol. **137**, 201–219 (1997).
[39]*The Handbook of Chemistry and Physics*, edited by D. R. Lide (CRC Press, 2004).
[40]S. Chandrasekhar, *Hydrodynamic and Hydromagnetic Stability* (Clarendon Press, Oxford, 1961).
[41]H. Emami-Meybodi, "Stability analysis of dissolution-driven convection in porous media," Phys. Fluids **29**, 014102 (2017).
[42]J.-P. Caltagirone, "Stability of a saturated porous layer subject to a sudden rise in surface temperature: Comparison between the linear and energy methods," Q. J. Mech. Appl. Math. **33**, 47–58 (1980).
[43]S. F. Shen, "Some considerations on the laminar stability of time-dependent basic flows," J. Aerosp. Sci. **28**, 397–404 (1961).
[44]M. C. Kim, C. K. Choi, and D.-Y. Yoon, "Relaxation on the energy method for the transient Rayleigh–Bénard convection," Phys. Lett. A **372**, 4709–4713 (2008).
[45]Y. H. Kim and M. C. Kim, "Relative energy stability analysis on the onset of Taylor-Görtler vortices in impulsively accelerating couette flow," Korean J. Chem. Eng. **31**, 2145–2150 (2014).
[46]J. Colombani and J. Bert, "Holographic interferometry study of the dissolution and diffusion of gypsum in water," Geochim. Cosmochim. Acta **71**, 1913 (2007).
[47]P. M. Gresho and R. L. Sani, "The stability of a fluid layer subjected to a step change in temperature: Transient vs. frozen time analyses," Int. J. Heat Mass Transfer **14**, 207–221 (1971).
[48]B. Miquel and K. Julien, "Hybrid Chebyshev function bases for sparse spectral methods in parity-mixed PDEs on an infinite domain," J. Comput. Phys. **349**, 474–500 (2017).
[49]M. C. Kim, H. K. Park, and C. K. Choi, "Stability of an initially, stably stratified fluid subjected to a step change in temperature," Theor. Comput. Fluid Dyn. **16**, 49–57 (2002).
[50]G. Balestra, P.-T. Brun, and F. Gallaire, "Rayleigh-Taylor instability under curved substrates: An optimal transient growth analysis," Phys. Rev. Fluids **1**, 083902 (2016).
[51]G. Balestra, M. Badaoui, Y.-M. Ducimetière, and F. Gallaire, "Fingering instability on curved substrates: Optimal initial film and substrate perturbations," J. Fluid Mech. **868**, 726–761 (2019).
[52]F. Haudin, L. A. Riolfo, B. Knaepen, G. M. Homsy, and A. de Wit, "Experimental study of a buoyancy-driven instability of a miscible horizontal displacement in a Hele-Shaw cell," Phys. Fluids **26**, 044102 (2014).
[53]J. Guo, F. Laouafa, and M. Quintard, "A theoretical and numerical framework for modeling gypsum cavity dissolution," Int. J. Numer. Anal. Methods Geomech. **40**, 1662–1689 (2016).